



# CONTROLS OF THE GEOMETRY AND EVOLUTION OF SALT DIAPIRS IN EXPERIMENTAL MODELS AND NATURAL EXAMPLES

Shankar Mitra and Pierre Karam

*School of Geology and Geophysics, University of Oklahoma, 100 E. Boyd St., Norman, Oklahoma 73019, U.S.A.*

## ABSTRACT

The geometry and evolution of salt diapirs are dependent primarily on the rates of sedimentation ( $R_a$ ) and salt flow ( $R_{sg}$ ). Experimental models were conducted to study the controls of sediment load, sedimentation rate, and thickness of the source layer on the geometry and evolution of diapirs. The experiments used both constant and variable sedimentation rates, and different thicknesses of silicone gel, representing salt. Constant sedimentation rate experiments show that larger loads, lower rates of sedimentation and thicker source layers result in higher  $R_{sg}$  to  $R_a$  ratios leading to cylindrical diapirs, which eventually develop flared shapes with overhangs, whereas smaller loads, higher sedimentation rates and thinner source layers result in lower  $R_{sg}$  to  $R_a$  ratios leading to tapered shapes and eventual eclipse and occlusion of the diapirs. Variable sedimentation rates result in changing shapes of diapirs over time. A small increase in sedimentation rates for flared or cylindrical diapirs result in an initial eclipse followed by tapering and a transition to active diapirism, enabling the diapir to pierce the overlying sediments and continue to grow by passive diapirism. A large increase in sedimentation rates result in a permanent eclipse, because the tapered diapir is unable to penetrate the larger thickness of the overburden.

The models suggest that tapering and flaring are mechanisms for maintaining an equilibrium between net rates of sedimentation ( $R_a$ ) and salt rise ( $R_{sn}$ ), with changing  $R_{sg}/R_a$  values. Flaring is caused by high  $R_{sg}/R_a$ , but is also an effective mechanism of decreasing the rate of net salt rise by increasing the surface area of the top of the diapir. Tapering is caused by low  $R_{sg}/R_a$ , but is also a mechanism for increasing the rate of salt rise by decreasing the diameter. The results of the experimental models can be used to understand the geometry and evolution of natural diapirs. The models are directly applicable to analyzing the geometry and evolution of poorly or partially imaged salt diapirs in salt basins.

In the East Texas Basin, diapirs located on the basin flanks, such as the Bethel and Oakwood domes are characterized by small diameters and salt volumes, likely related to a relatively thin source layer. They exhibit cylindrical to flared geometries followed by rapid tapering and flattening of the top of the diapir due to increased sedimentation rates. On the other hand, diapirs located along the central basin axis such as the Butler and Stein domes are characterized by larger diameters and salt volumes, because of a thicker source layer. They exhibit early cylindrical to flared patterns, but also show earlier tapering of the top, suggesting the effects of a depleted source layer, during the later stages of their evolution.

## INTRODUCTION

Salt diapirs form by a number of mechanisms (Jackson et al., 1994; Hudec and Jackson, 2007), including (Fig. 1): (1) active diapirism, if the salt deforms and eventually pierces the faulted overlying sediments (Trusheim, 1960; Bishop, 1978; Nettleton, 1934; Schultz-Ela et al., 1993); (2) passive diapirism, if the salt movement is primarily influenced by the downbuilding of overlying sediments (Barton, 1933; Talbot, 1995), and (3) reactive diapirism, if the salt moves primarily in response to faulting induced by regional extension (Vendeville and Jackson, 1992a). It is now

widely believed (for example, Jackson et al., 1995) that diapirs grow by passive diapirism for most of their evolutionary history, with active and reactive diapirism occurring as secondary mechanisms.

The shapes of diapirs, as defined by the interface angle ( $\alpha$ ) between the sediments and the salt, are dependent primarily on the rates of aggradation of sediments and salt flow (Talbot, 1995). Talbot (1995) related  $\alpha$  to the net rate of aggradation ( $R_a$ ) and net rate of vertical salt rise ( $R_s$ ). In fact, the key parameters are the gross rate of salt rise ( $R_{sg}$ ), defined as the incremental volume of salt passing through a unit area, and the rate aggradation ( $R_a$ ) defined as the incremental volume of sediments deposited over a unit area (Fig. 2A), so that:

$$\tan(\alpha/2) = R_{sg}/R_a \quad (\text{Eq. 1})$$

On this basis, the shapes of salt/sediment boundaries can be classified as tapering, cylindrical, and flaring (Fig. 2B).

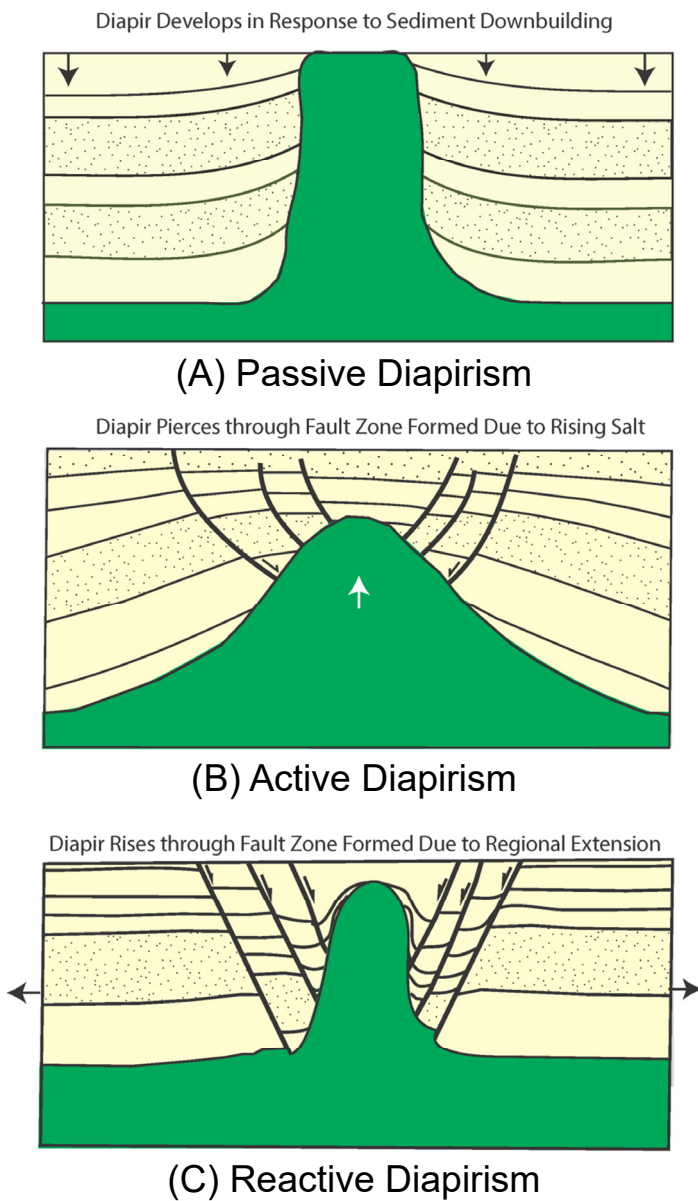
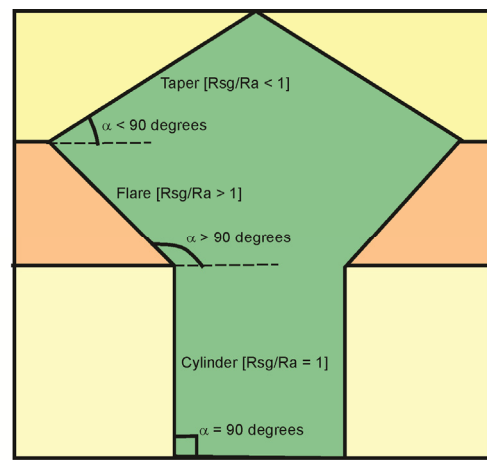


Figure 1. Main mechanisms of diapir formation: (A) passive diapirism, with the growth of the diapir due to sediment down building (based on Barton, 1933); (B) active diapirism, with the diapir piercing through sediments faulted by the rising salt; and (C) reactive diapirism, with the diapir rising through a fault zone formed by regional extension (modified after Vendeville and Jackson, 1992).

Examples from the Gulf of Mexico and the East Texas Basin suggest that diapirs commonly exhibit a combination of these three shapes suggesting variations in the relative rates of aggradation and salt flow. Although average sedimentation rates can be approximately determined in many basins, the rate of gross salt rise is dependent on a number of factors, and is generally more difficult to estimate.

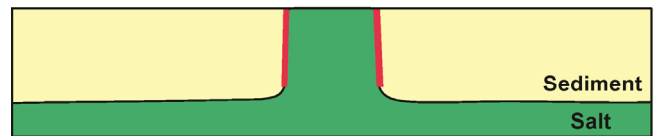
In this paper, we conduct experimental models to study the controls of some key factors controlling the rates of salt flow. This enables an improved understanding of the resulting geometry and evolution of salt diapirs, and conditions resulting in the transition from passive to active diapirism. The experiments use both constant and variable sedimentation rates, and different thicknesses of silicone gel, representing salt.

The experimental models are compared with some well documented natural examples of diapirs from the East Texas Basin,



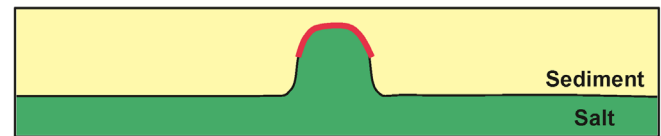
A  $R_{sg}/R_a = \tan(\alpha/2)$

$R_{sg} = R_a$



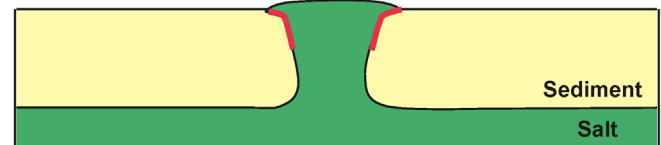
Cylinder

$R_{sg} < R_a$



Taper

$R_{sg} > R_a$



Flare

Figure 2. (A) Relationship between the salt/sediment boundary angle ( $\alpha$ ), and the ratio of gross salt flow rate ( $R_{sg}$ ) and the rate of aggradation ( $R_a$ ). (B) Schematic figure showing the three main configurations of salt/sediment boundaries based on the  $R_{sg}/R_a$  ratio (based on Talbot, 1995).

documented by Wood and Giles (1982) and Seni and Jackson (1983a, 1983b). The results of the experimental models provide some insights regarding the possible reasons for the variation in diapir shapes in the East Texas Basin.

### EXPERIMENTAL APPROACH

Experimental models were used to study the effects of different factors influencing salt movement. The main factors studied were sediment thickness, sedimentation rate, and source layer thickness.

The materials used were silicone gel, with a viscosity of  $10.1 \times 10^{-4}$  Pa sec, and a density of  $0.9 \text{ gm/cm}^3$  to represent the salt, and garnet sand, with a density of  $4 \text{ gm/cm}^3$  to represent the sediments. Assuming that salt behaves as a Newtonian or power law fluid over geological time, the silicone gel serves as a good analog within the time limit of the experiments (Weijermars et al., 1993). Salt-sediment interactions involving diapirism and fault-salt interactions have used silicone gel to represent salt and silica sand to represent sediments, and have successfully simulated natural structures (Vendeville and Jackson 1992a, 1992b; Ge et al., 1997; Brun and Fort, 2011; Warsitzka et al., 2013). The density ratio between sand and silicone gel is higher than found in natural environments, resulting in overestimating the role of buoyancy, and this effect is exacerbated for garnet sand. However, it reduces the length of the experiments and reduces the inefficiencies associated with trying to deposit thin but uniform layers of sand over long periods of time. The effects of density inversion with depth is also not represented in this and previous models, because unlike natural structures, the sand in the models undergoes no effective compaction. Because the purpose of our experiments is primarily to investigate the relative variations introduced by changes in the parameters, the effects of inaccurate scaling are not as significant. A good review of considerations in developing experiments models is provided in Johnson (1970).

Experiments were run in a 30 cm x 15 cm sand box to avoid edge effects. The silicone gel was initially loaded by 0.5 cm of sand on the sides, leaving a 1 cm groove in the middle with no deposition, to enable the silicone to rise. A small pillow with its top at the surface developed. In natural examples, this initial state will develop by a combination of passive and active diapirism or by reactive diapirism. The system was then progressively loaded with a total sand thickness of 4.5 cm. A variable test duration was used, depending on the sedimentation rate. Therefore, the individual layers marked in the figures represent different time periods, depending on the rate of sedimentation. Upon the completion of the experiment, the sand was saturated with water and cross-sections were cut every 1 cm parallel to the longest box dimension to examine the shape of the diapir and the structural deformation of the beds around it.

A series of controlled experiments was used to study the influence of: (1) the thickness of the sedimentary column, (2) the depositional rate, and (3) the thickness of the source layer on salt diapir geometry. Some experiments were conducted with variable rates to study how diapirs change shape with changes in the rates of sedimentation.

Depositional thicknesses and rates were recorded, and changes in the shapes of the diapirs were analyzed during the experiments. Comparison between the dimensions of the structures observed in photographs taken from the top and in serial cross sections cut at the end of the experiment were used to study the changes in the shapes of the diapirs. Because the shape of the salt diapir varied along trend, suggesting movement of the salt out of or into each section, the area of salt was not balanced in each section. For each experiment, the cross section with the most mature geometry was selected to study the evolution.

## EXPERIMENTAL RESULTS

Both constant and variable sedimentation rate experiments were designed to study the influence of the following parameters on the salt flow rate and resulting diapir geometry: (1) the sedimentation rate, (2) the sediment load as defined by the thickness of the overburden sediments, and (3) the thickness of the source layer. The results are presented as comparisons between different experiments to illustrate the controls of these factors.

## Experiments with Constant Sediment Rates

### Rates of Sedimentation and Differential Sediment Load

Experiments G2 and G3 studied the impact of sedimentation rates for a constant sediment load. These experiments had the same thickness of the silicone layer (1 cm), but used different rates of constant rate sedimentation (0.25 and 0.5 cm/hr, respectively).

In experiment G2 (Fig. 3), deposition of sand at the pre-defined rate of 0.25 cm/hr, resulted in the silicone gel moving to the surface during the initial phase forming a ridge with vertical walls. Subsequently individual diapirs separated and grew by widening at the surface, without significant burial of the top of the silicone.

The growth of the diapir was passive with the silicone surface remaining at the surface with a progressive increase of the diameter, implying an increasing rate of gross salt flow compared to the rate of deposition in spite of a constant sedimentation rate, due to the increasing sediment load. The relatively low sedimentation rates (0.25 cm/hr) resulted in continuing passive diapirism with a transition from a cylindrical to flared geometry over time. Characteristic rim synclines with the sand thickness increasing into the salt diapir formed due to evacuation of the salt from the surrounding areas. During the later stage of diapirism, the salt flow resulted in upturn of the sediments in the vicinity of the diapir boundary.

In experiment G3, which had a higher sedimentation rate of 0.5 cm/hr (Fig. 4), a small pillow developed, which was quickly eclipsed after the deposition of the second sand layer. The dimensions of the diapir did not change from this time to the end of the experiment, implying that no additional movement occurred in the subsurface. The higher rate of sedimentation eclipsed the silicone at a very early stage and suppressed further rise, resulting in a tapered shape of the top of the silicone. These experiments confirm the delicate balance between sedimentation rates and differential sediment load in controlling the salt flow.

Experiment G2 shows the effect of depositional load on the rate of salt flow, for a constant rate of sedimentation. The rate of sedimentation was low enough for the rate of salt rise to keep pace with the rate of sedimentation. With a constant low rate of sedimentation, the increasing sediment load results in a transition from cylindrical to flared geometries, suggesting progressively increasing rates of salt flow. On the other hand, the higher rate of sedimentation in G3 results in a tapered geometry and early eclipse of the diapir.

### Source Layer Thickness

Experiments G1 and G2 used different thicknesses of silicon (0.75 and 1.00 cm, respectively), but the same rate of sedimentation (0.25 cm/hr) to study the influence of the original salt-layer thickness.

In experiment G1 (Fig. 5), constant rate sedimentation resulted in the pre-existing ridge being covered and reduced in size to a diapir with a narrow diameter. The diapir remained at the surface during the early stages, but was subsequently buried. The growth of the diapir changed from a passive to an active mechanism after burial and stopped beyond a critical sediment load. The source layer of silicone gel was not evacuated completely at the end of the experiment. The reduced rate of flow into the diapir is due to frictional resistance between the basal plate and the overlying sand and the silicone, suggesting that salt flow decreases before complete evacuation and the formation of a salt weld.

On the other hand, experiment G2 (Fig. 3), which had a greater initial thickness of 1 cm of the silicone layer developed a flaring and emerging diapir, with an increasing width of the diapir over time.

A comparison of experiments G1 and G2 shows the control of source layer thickness on salt flow. Because both G1 and G2

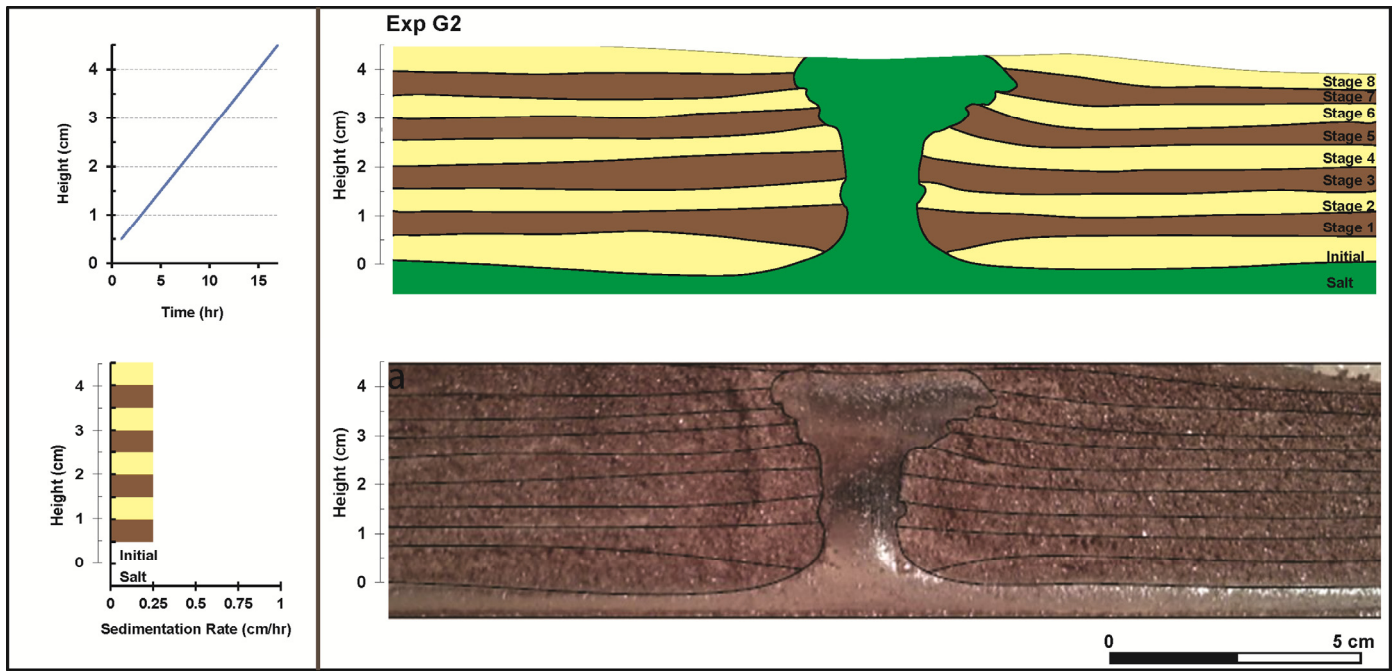


Figure 3. Experimental results for G2 (garnet sand), with an initial thickness of silicone of 1 cm, and a constant deposition rate of 0.25 cm/hr. The diapir progresses from a cylindrical to a flared geometry. Cross sectional sketch of final geometry of silicone diapir and a photograph with the final geometry are both shown in this and other figures showing the experimental results. Graphs to the left show the change in sediment load and deposition rate over time. In this and other figures showing experimental results, the graph of the sedimentation rate and load shows the final thickness of the silicone gel observed in the cross sections. Initial refers to the pre-kinematic sand thickness.

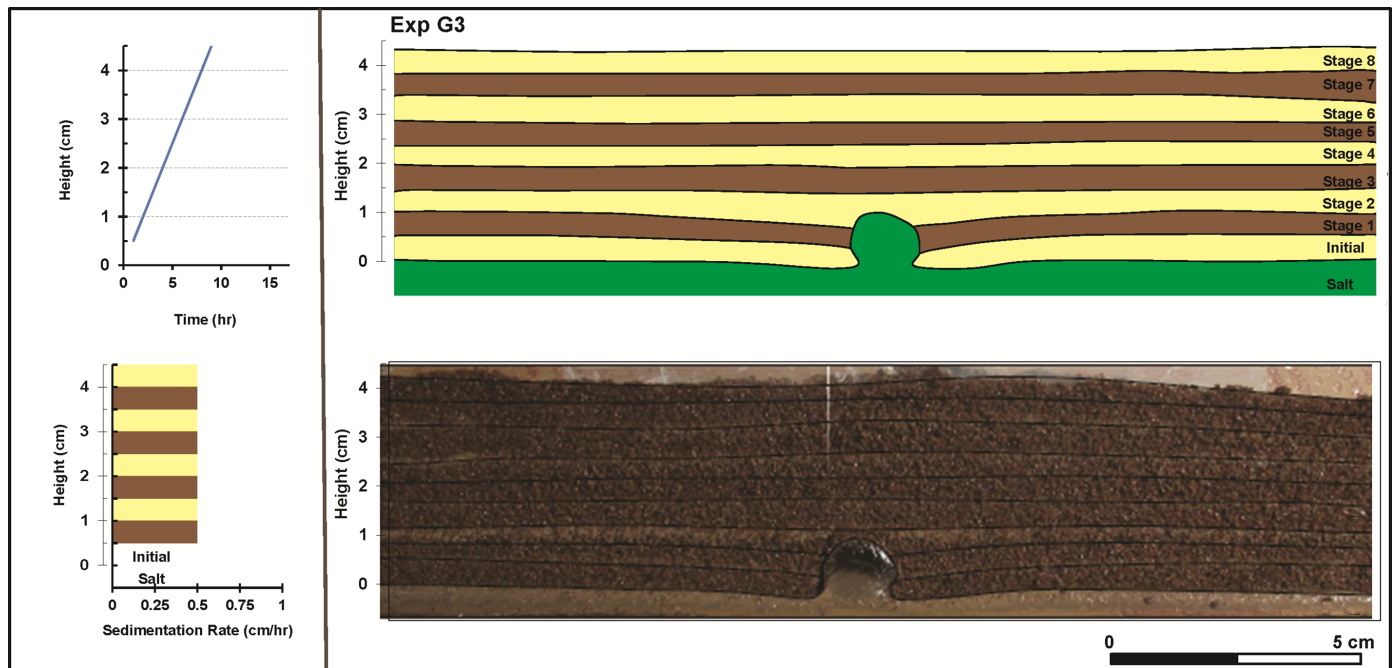
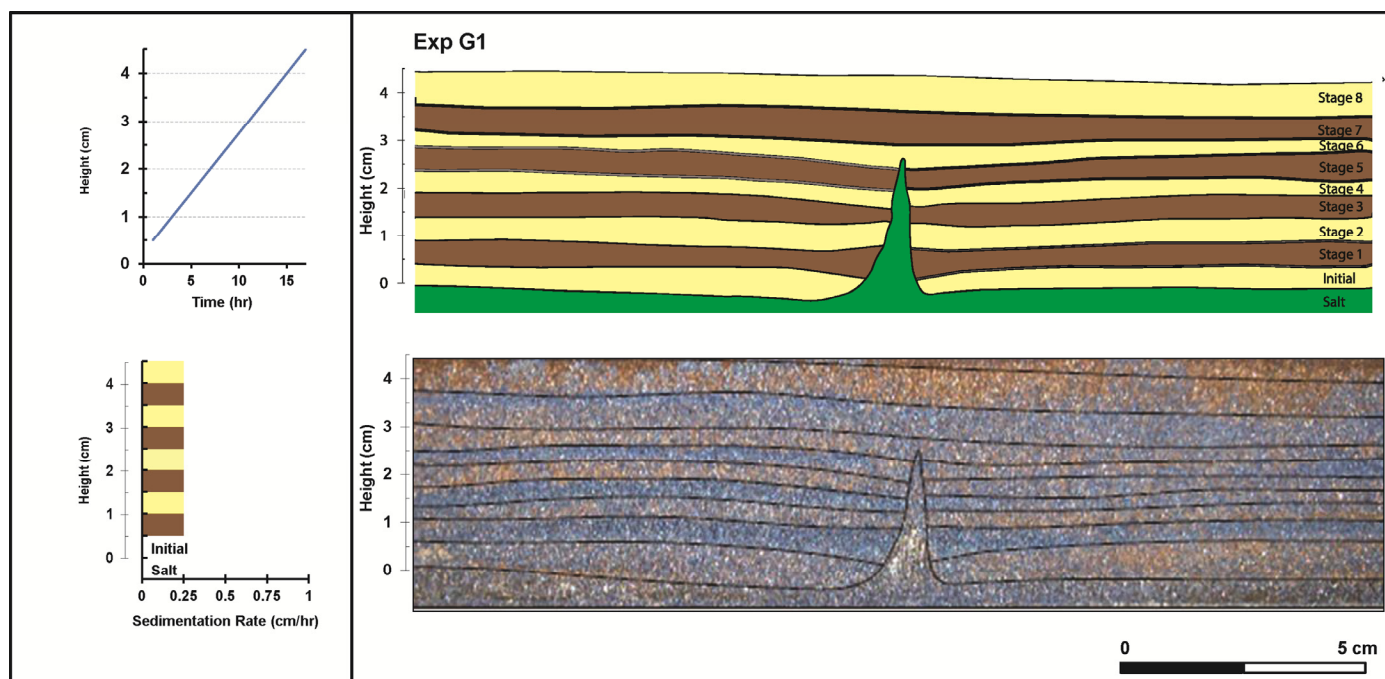


Figure 4. Experimental results for G3, with an initial thickness of silicone of 1.0 cm and a constant deposition rate of 0.5 cm/hr. The diapir develops a taper and is eventually eclipsed, as a result of the high sedimentation rate.

had the same loading history, it is inferred that the greater initial silicone thickness in G2 resulted in higher rates of salt flow and continued passive diapirism, whereas the smaller initial thickness of silicone in G1 resulted in early eclipse and eventual occlusion of the diapir. Furthermore, both the volume of salt in the diapir and the diameter of the diapir was significantly larger in experiment G2 due to the greater thickness of the salt layer.

### Experiments with Variable Rates of Sedimentation

Experiments conducted with variable rates of deposition were used to study the effects of changing sedimentation rates (G6–G8), and also the thickness of the source layer. The rate of deposition was increased after deposition of half the total height of the sediments. The controls of different pairs of depositional



**Figure 5. Experimental results for G1, with an initial thickness of silicone of 0.75 cm and a constant deposition rate of 0.25 cm/hr. The thin source layer results in a narrow diapir that is eventually eclipsed.**

rates (G6, and G7), and the thickness of the source beds (G6 and G8), were studied.

#### Changes in Sedimentation Rates

G6 and G7 had an initial silicon gel thickness of 1 cm, but a variable sedimentation rate that increased from 0.25 cm/hr to 0.5 cm/hr and 1.0 cm/hr, respectively. During the deposition of the first 2 cm at a rate of 0.25 cm/hr in G6 (Fig. 6), the silicone formed a ridge, which eventually developed into a flare due to the increased load. As the deposition rate increased to 0.5 cm/hr, a large part of the structure was covered. However, with the increase in loading, the diapir tapered to a narrower diameter and reached the surface. Passive diapirism was interrupted for a short period when the diapir was covered and the silicone had to pierce the crest to reach the surface through active diapirism.

Experiment G7 (Fig. 7) was marked by a larger increase in deposition rate from 0.25 cm/hr to 1 cm/hr. The sudden increase in sedimentation rate to 1 cm/hr during the second phase caused the diapir to be totally eclipsed. The diapir remained eclipsed and was eventually occluded towards the end of the experiment. This experiment revealed the importance of a sudden increase in sedimentation rate as a restraining element that prevents growth of the diapir.

A comparison of experiments G6 and G7, shows that in experiment G6, a small increase in depositional rate eclipsed the diapirs for a short period of time. During this period the diapirs tapered and continued their upward rise to the surface through active diapirism before returning to the passive mechanism again. Tapering effectively decreased the diameter and increased the curvature of the contact with the overlying sand, allowing the diapirs to adapt by rising at a higher net rate.

On the other hand, in experiment G7, the rapid increase in the rate of deposition also caused the diapir to taper, but the silicone was unable to pierce the thicker sediment load and stopped moving. These experiments reveal the delicate balance between increasing sediment load, which tends to increase salt flow rates, and increasing sedimentation rate, which tends to restrain movement.

#### Source Bed Thickness

Experiment G8 (Fig. 8) shows the effects of source bed thickness on diapir growth under varying depositional rates. This experiment used the same pair of deposition rates for the two stages of diapir growth (0.25 and 0.5 cm/hr, respectively) as experiment G6, but had a greater source bed thicknesses of 1.5 cm. In G8 (Fig. 8), The mechanical behavior of the diapir was similar to G6 in that the first stage is characterized by a purely passive mechanism, followed by a tapering phase, which enabled active diapirism for the top of the silicone to return to the surface. The final geometry consisted of two stacked flared diapirs formed during the two stages. The main difference was a higher gross flow rate resulting in a wider diapir and a significantly higher diapir volume in both stages, largely due to the greater thickness of the silicone layer.

G6 and G8 show the influence of source bed thickness on the flow rates and diapir shapes. This is reflected in the increased changes in the diameter and volume of the diapir. Thicker source beds result in higher flow rates and wider diapirs or sheets, and this in turn controls the geometry and mechanisms of active diapirism during the second stage.

#### Relationship of Diapir Shapes to Salt and Sediment Rates

Diapir shapes are related to the variation in gross rates of salt flow ( $R_{sg}$ ) and aggradation ( $R_a$ ), and the tendency for the net rise of the salt ( $R_{sn}$ ) to be in equilibrium with sedimentation rates (Fig. 9). Equilibrium is maintained as long as the top of the salt remains at the surface and is only disturbed during emergent flow of the salt, or burial. Flaring results from increasing  $R_{sg}$ , with constant  $R_a$  or decreasing  $R_a$  with constant  $R_{sg}$  (Figs. 9A and 9B). Other possibilities with both  $R_{sg}$  and  $R_a$  rising or falling are also possible, as long as the ratio of  $R_{sg}/R_a$  is greater than 1. Similarly, tapering results from decreasing  $R_{sg}$  with constant  $R_a$ , increasing  $R_a$  with a constant  $R_{sg}$  (Figs. 9C and 9D), or other conditions where  $R_{sg}/R_a$  is less than 1.

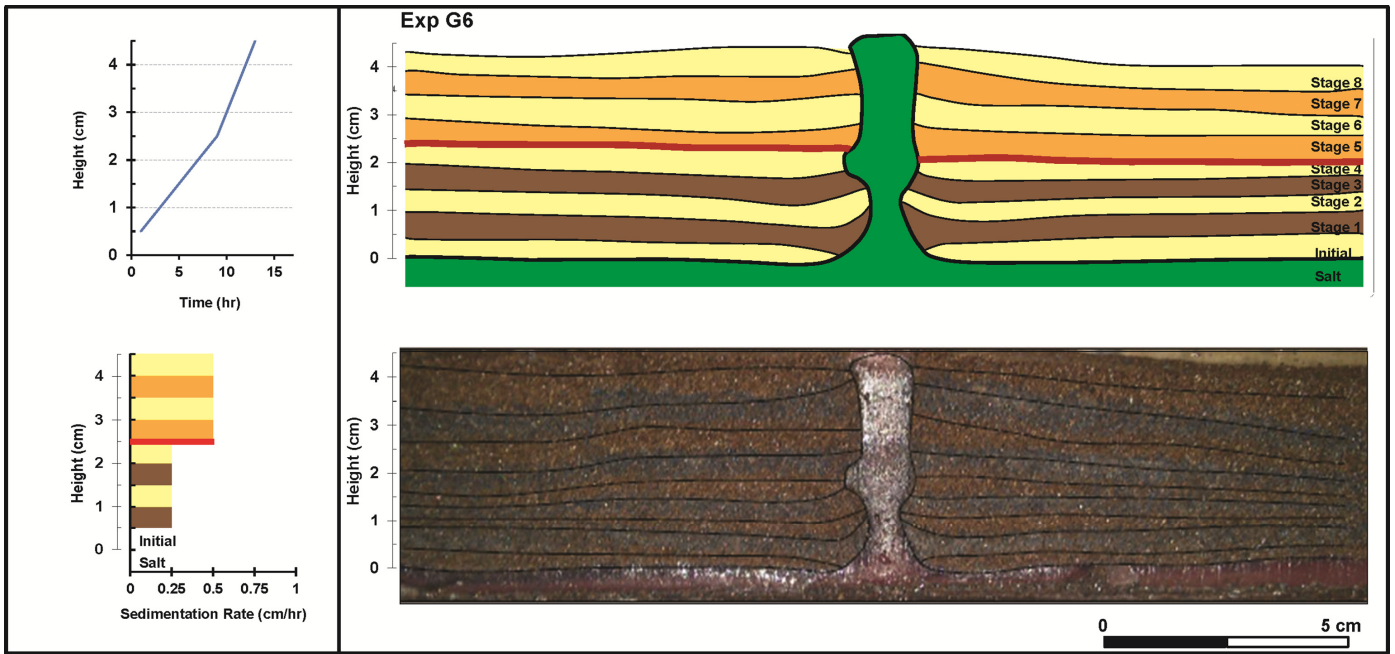


Figure 6. Experimental results for G6, with an initial thickness of silicone of 1 cm and a deposition rate of 0.25 cm/hr changing to 0.5 cm/hr in the middle of the experiment. This results in a taper with the increase in sedimentation rate, followed by active diapirism, emergence of the diapir, and its rise with a cylindrical geometry.

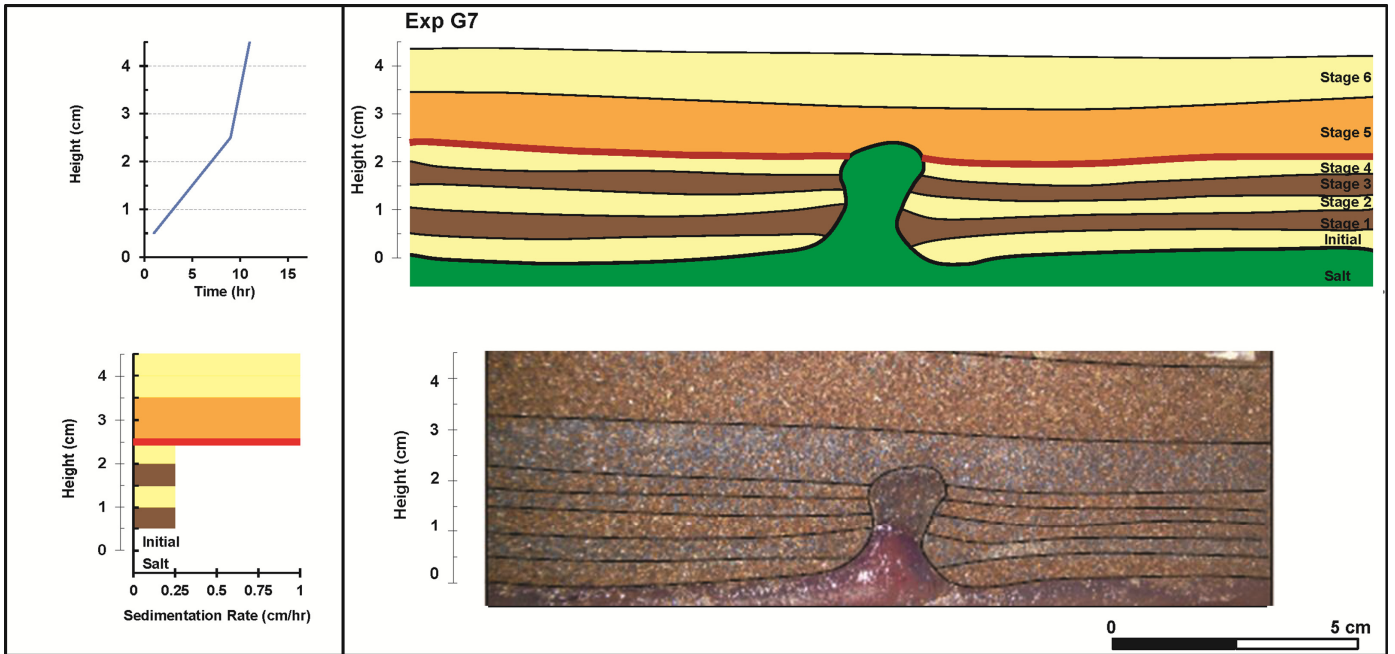
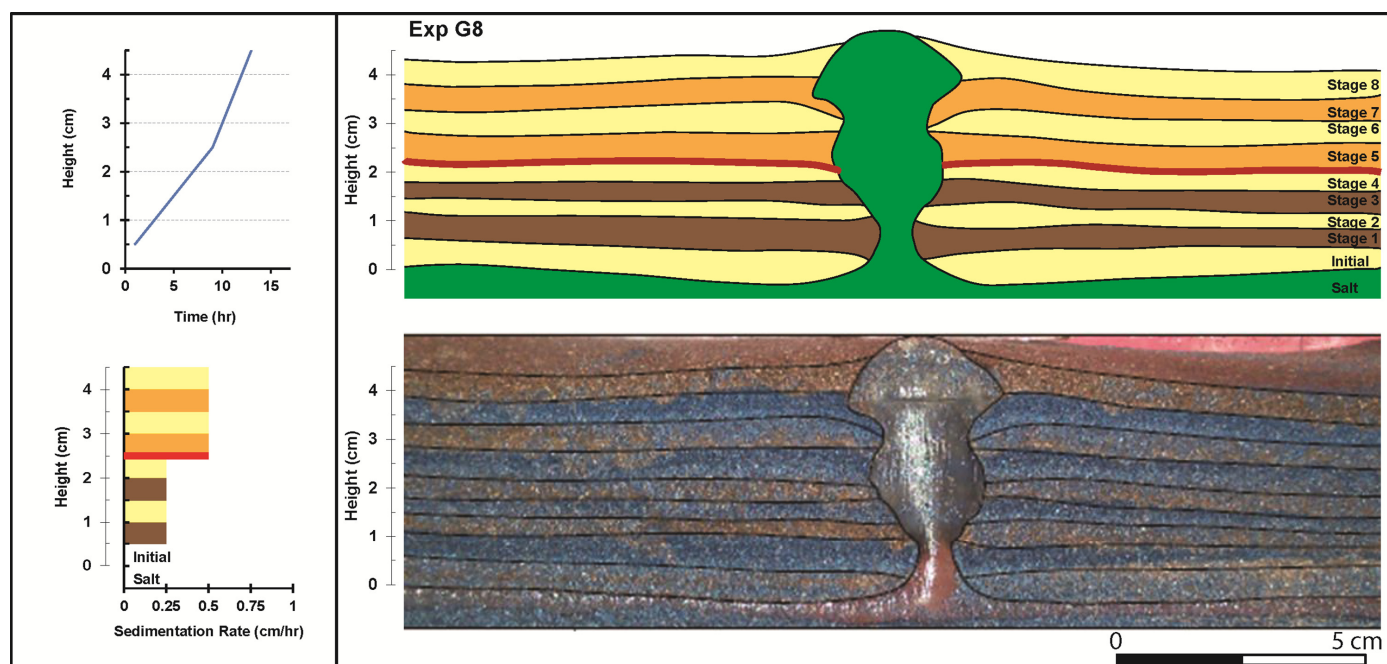


Figure 7. Experimental results for G7, with an initial thickness of silicone of 1 cm and a deposition rate of 0.25 cm/hr changing to 1.0 cm/hr in the middle of the experiment. The diapir is eclipsed due to the large increase in depositional rate.

Flaring results in an increase in the diameter and area of the top of the diapir, thereby the velocity of salt rise. Tapering, on the other hand, results in a decrease in the diameter, thereby increasing the rate of net rise of the salt. These effects are observed in the constant rate experiments, with the development of flared shapes with increasing rates of gross salt flow (G2), and tapered or spindle shapes with decreasing rates of gross salt flow

(Gland G3). Variable rate experiments show the tapering of the diapirs with increasing rates of aggradation and the resulting decreasing rates of gross salt flow. Tapering reduces the surface area of the top of the diapir, thereby increasing the pressures, and enabling the salt to rise at a higher rate by active processes to reach the surface (G6 and G8) and continue growing by a passive mechanisms.



**Figure 8.** Experimental results for G8, with an initial thickness of silicone of 1.25 cm and a deposition rate of 0.25 cm/hr changing to 0.5 cm/hr in the middle of the experiment. The greater thickness of the source layer results in a wider diapir with a larger volume at both stages.

## COMPARISON WITH NATURAL EXAMPLES

Diapirs from a number of salt basins display all of the geometries observed in the experiments. The evolutionary history of these diapirs is more difficult to analyze, but comparisons with the experimental models provide insight into the possible evolution and controls of salt flow rates. The upward transition from cylindrical to flared shapes with constant sedimentation rates observed in experiment G2 is a common geometry observed, for example, in the Wienhausen Diapir from the Northwest German Basin (Gussow, 1968), and in a number of diapirs from the Gulf of Mexico, including the Main Pass Block 299 Field. The Bethel and Oakwood diapirs in the East Texas Basin (Wood and Giles, 1982), also display this geometry. In some of these examples, the extent of flaring may be enhanced by an upward decrease in the rate of sedimentation.

A number of examples of eclipsed and occluded diapirs, which result either from rapid increase in sedimentation rates (experiment G3) or by depletion of the salt source (experiment G1), are seen in the East Texas Basin including the Butler, Steen, and Boggy Creek diapirs (Wood and Giles, 1982; Jackson and Seni, 1984; Talbot, 1995). Some of these examples display tapered geometries of the top of the diapir. Finally, stacked diapirs with alternating tapered and flared geometries suggestive of variations in deposition rates (experiments G6 and G8) have been reported from the North Sea (Jenyon, 1986; Talbot, 1995), although these are usually poorly imaged on seismic.

An important observation for a number of the experiments was that initial movement of salt resulted in the formation of ridges rather than individual diapirs. Continued loading resulted in the development of separation of two or more diapirs from the ridges. This implies that initial lateral movement of the salt was followed by longitudinal movement, possibly driven by small differences in the rate of loading along the ridge. Therefore, there is significant movement of salt out of the plane of the cross sections, so that the area of salt in individual sections cannot be balanced, and a volumetric balance of the entire system is necessary. These results are in agreement with observations by

Trusheim (1960) for salt structures in Northwest Germany, and the East Texas Basin (Seni and Jackson, 1983a, 1983b). An example of a mapped structure from offshore Louisiana that consists of multiple diapirs developed from a single ridge is the Bay Marchand Salt Ridge (Frey and Grimes, 1970).

## EAST TEXAS BASIN

We focus on a few salt diapirs from the East Texas Basin to see how the experimental results can be used to understand the controls of salt flow rates and the final diapir geometries.

### Regional Geology and Evolution

The East Texas Basin is bounded by the Mexia-Talco Fault Zone to the northwest and the Mount Enterprise Fault Zone to the southeast (Fig. 10). The basin is a failed rift basin and comprises one of several inland basins in Texas, Louisiana and Mississippi, which were connected with the Gulf of Mexico during a significant part of their evolutionary history, but were isolated from the Gulf of Mexico with cessation of sedimentation in Paleogene time. The Jurassic Louann salt was deposited as part of the post-rift complex over the Triassic rift fill, and is believed to be thickest in the central part of the basin. Following its deposition, the salt was overlain by platform carbonates of the Jurassic Smackover-Gilmore, and siliciclastic deposits of the Schuler-Hosston in the late Jurassic to early Cretaceous (Seni and Jackson, 1983a). This was followed by alternating deposits of carbonate and siliciclastic sediments, with termination of sediment infill in Oligocene time. Overall, the sediment infill and the Louann salt are thickest in the central part of the basin. As a result, some of the most mature and larger salt diapirs are located in the central part of the basin, whereas the rims of the basin are marked by salt pillows and smaller diapirs.

### Rates of Sedimentation and Gross Salt Flow

For most of the basin, data of sediment infill and diapir geometry are available for the Glen Rose and younger units, ena-

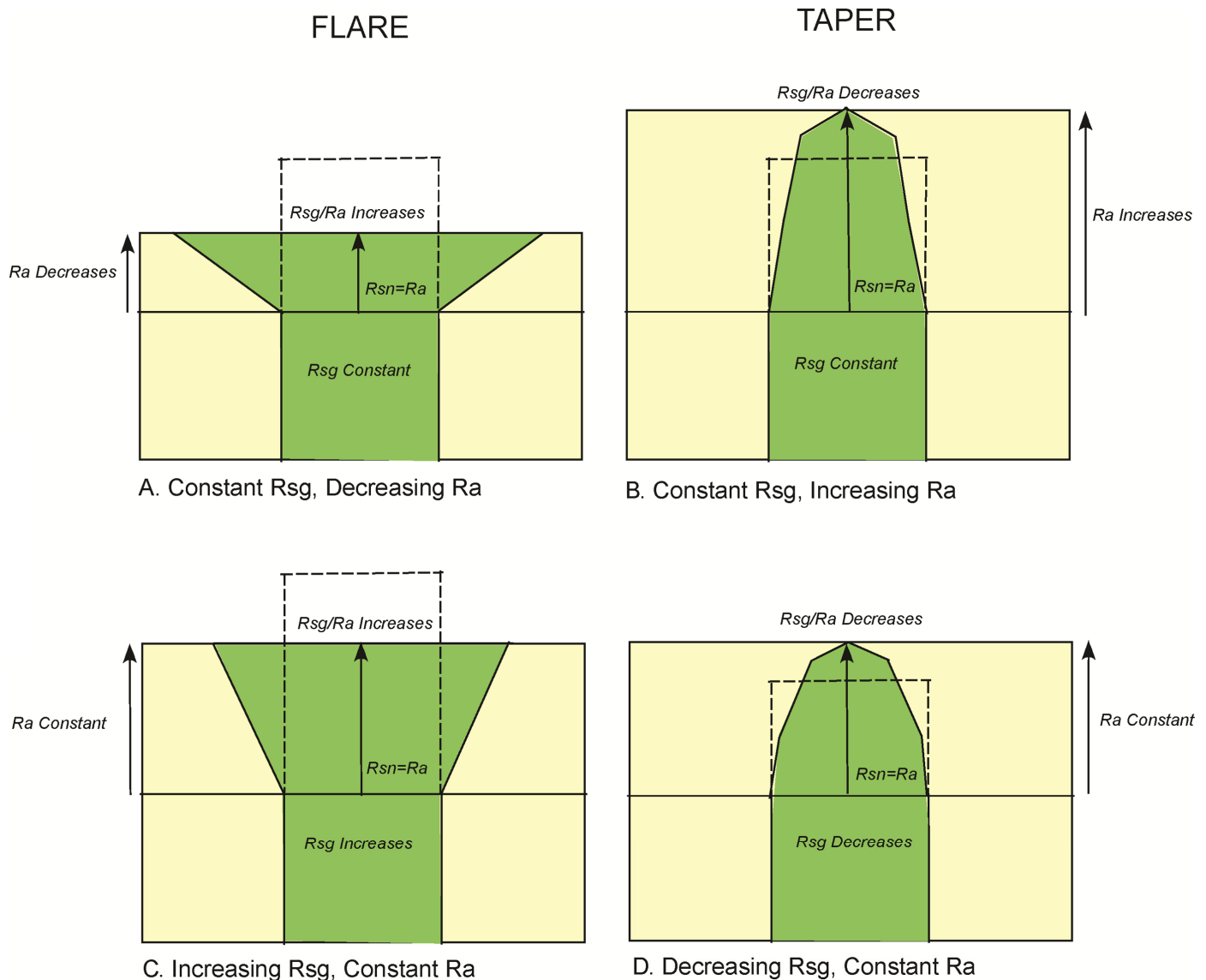


**Figure 9. Flaring and tapering as mechanisms of maintaining equilibrium between rates of aggradation ( $R_a$ ) and net salt rise ( $R_{sn}$ ). All figures are for equilibrium conditions. (A & B) Flaring induced by decreasing  $R_a$  (A) and increasing  $R_a$  (B). (C & D) Tapering induced by increasing  $R_{sg}$  (C) and decreasing  $R_{sg}$  (D). Non-equilibrium conditions will result in emergence and dissolution or eclipse of the diapir. See text for further discussion.**

bling a study of the timing and geometry of the diapirs (Wood and Giles, 1982; Jackson and Seni, 1984).

Average rates of sedimentation ( $R_a$ ) can be determined approximately by considering the thickness of different units and the time interval of their deposition, although the errors can be quite significant due to erosional events, variable compaction, and large variations in the rates of sedimentation within a unit. On this basis, it is apparent that within the basin, the rates were relatively high during the deposition of the Washita, Fredricksburg, and Eagle Ford groups (116–88.5 m.y.), dropped during the Austin/Tokio and Taylor chalks, Navarro marls, and Midway Group (88.5–59 m.y.) before rising sharply during the Wilcox-Claiborne groups (59–54 m.y.)

The rates of salt flow ( $R_{sg}$ ) are more difficult to determine. Seni and Jackson (1983b) attempted to measure rates of salt flow using a number of features, including: (1) thinning of strata above salt pillow, (2) volume of salt within each layer and (3) volume of salt evacuated from peripheral synclines. Using these approaches, they concluded that diapirs in the basin reached

the culmination of their diapiric activity at different times, based partly on their locations within the basin. Therefore, the variation in the rate of salt growth is more complex and appears to be related to multiple factors in addition to the thickness of the sediment column and the sedimentation rate.

### Geometry and Evolution of East Texas Diapirs

Diapirs within the East Texas Basin, show some important differences in size, salt volume and evolutionary history between those on the outer flanks and those in the center. These differences are related to changes in both the original thickness of the salt and the sedimentary column, both of which increase towards the center of the basin. Additional variation in each of these regions related to asymmetry and three-dimensional geometry also occur. In order to study the impact of some of the key factors driving salt diapirism, we study four representative diapirs, two on the flanks (Oakwood and Bethel) and two in the basin interior (Butler and Steen).

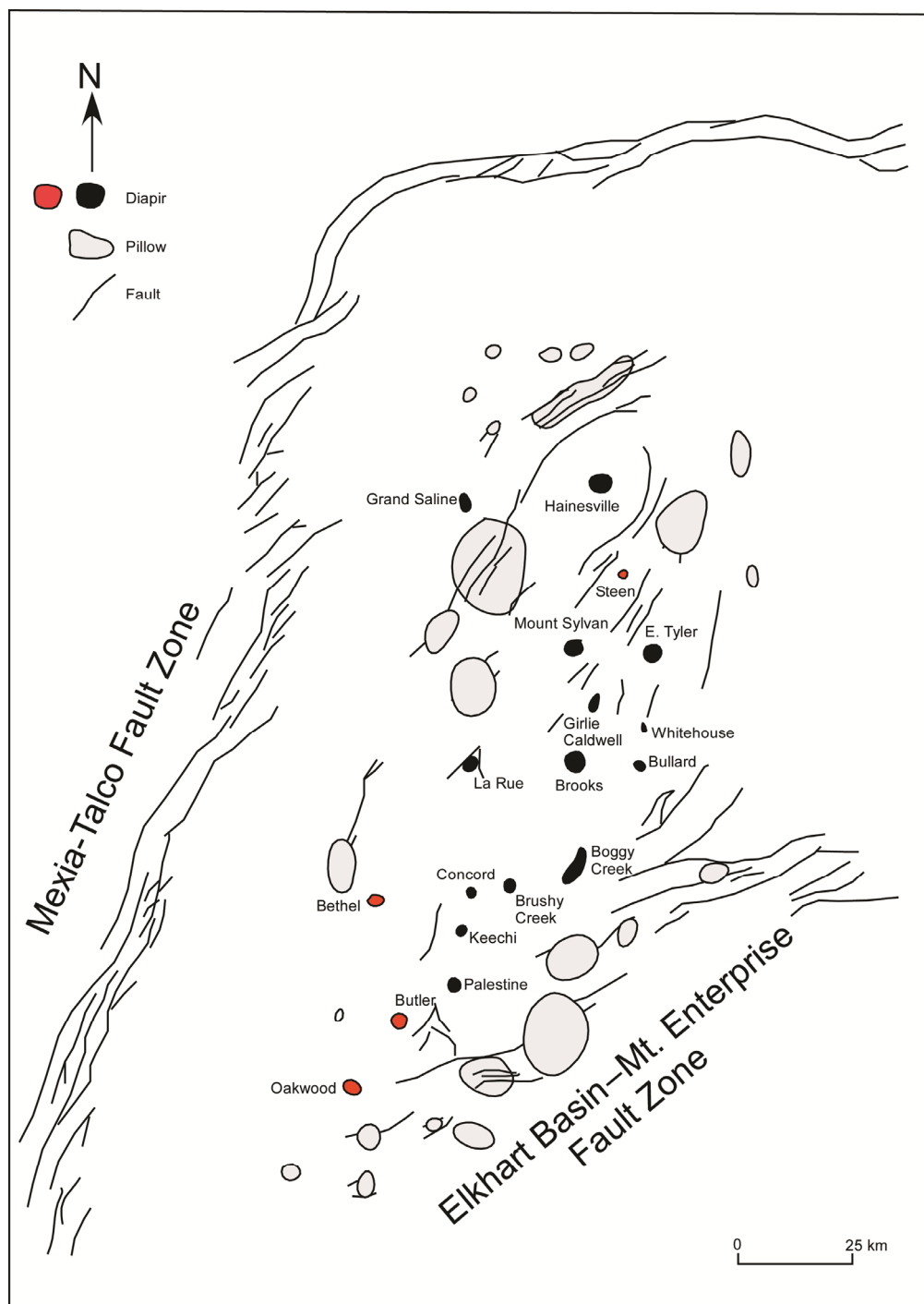


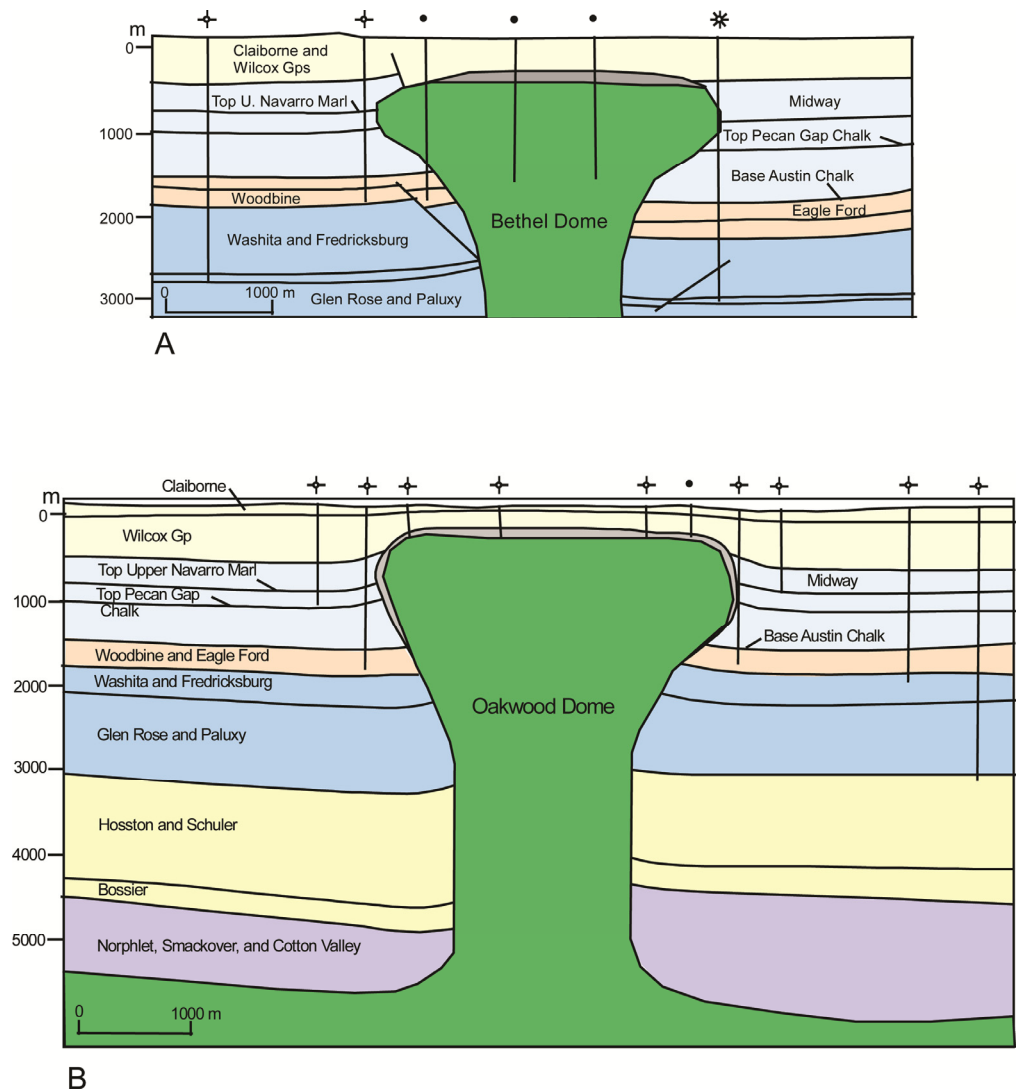
Figure 10. Generalized map of the East Texas Basin showing major salt pillows and diapirs (modified after Seni and Jackson, 1982b). Diapirs discussed in this paper are shown in red. The East Texas Basin is an elongated basin with a NNE-SSW trend. The Bethel Dome is located along the western margin, whereas the Oakwood Dome is located along the southwestern margin. The Steen and Butler domes are located along the approximate basin axis in the interior of the basin.

### Oakwood Dome

The Oakwood Dome is located along the southwestern margin of the basin (Fig. 10) and based on the data available, shows the most complete geometry of the diapir from its upper termination to the basal salt. The dome initiated with a tapered geometry in the Norphlet and Smackover (low  $R_{sg}/R_a$ ), consistent with an initial pillow geometry, and then developed a cylindrical geometry with an almost vertical wall ( $R_{sg}=R_a$ ) through the deposition of the Cotton Valley, Bossier, Hosston, and Schuler (Fig. 11A). During the early part of the deposition of the Glen Rose it developed a flared geometry ( $R_{sg}>R_a$ ), and maintained a constant salt/sediment boundary shape through the Paluxy, Washita, Fredricksburg, Woodbine, Eagle Ford, and the Cretaceous chalks

and marls. As shown in experiment G2 this upward flare can occur with almost constant sedimentation rates, simply due to the increase in sediment load which results in a higher  $R_{sg}$ . However, the lower  $R_a$  values during the deposition of the Cretaceous marls may have also exaggerated this effect, because lower  $R_a$  values result in flared geometries, even if  $R_{sg}$  is approximately constant. During the deposition of the Midway, the diapir shape returned through a vertical to slightly tapered geometry before significant tapering occurred within the Wilcox culminating in a flat top. The flattening in the Wilcox is likely related to higher sedimentation rates (experiment G7), or due to rapid depletion of salt in the source layer. Overall, the geometry of the Oakwood Dome is quite similar to that in experiment G2, but a constant deposition rate may not have been the only factor in the develop-

**Figure 11. Cross sectional geometries for two diapirs along the flanks of the East Texas Basin (modified after Wood and Giles, 1982). (A) Bethel Dome and (B) Oakwood Dome.**



ment of the final geometry, with changes in the sedimentation rate and depletion of the source layer, playing secondary roles.

### Bethel Dome

Bethel Dome is located along the western margin of the basin (Fig. 10). Only data for part of the Glen Rose and overlying units are available for this diapir. The geometry of the diapir above the Glen Rose almost exactly replicates that of the Oakwood Dome, with initial flaring between the Cotton Valley and the Cretaceous chinks followed by tapering in the Midway and flattening within the Wilcox (Fig. 11B). This implies a very similar evolutionary history.

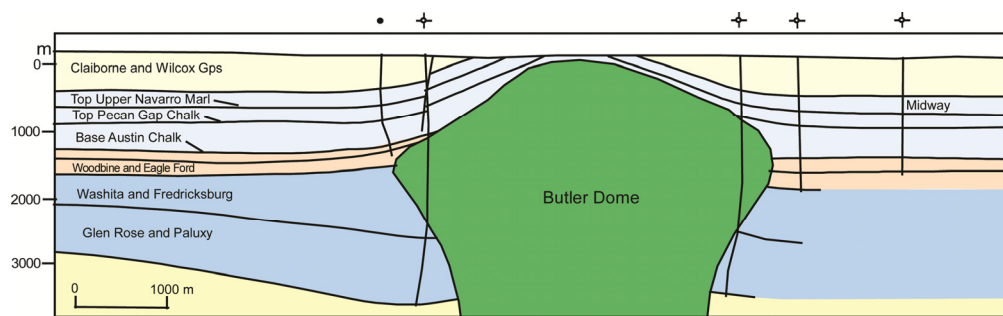
The Hainesville Dome on the northeastern margin of the basin (Loocke, 1978) shows a similar geometry to the Bethel and Oakwood domes. A common feature of the Bethel and Oakwood domes is their narrow diameter (typically 1200–1400 m) in the cylindrical feeder and small salt volume (area in cross section) in the Glen Rose and higher units, compared to diapirs in the center of the basin. This is most likely related to the thinner source layer along the flanks of the basin.

### Butler Dome

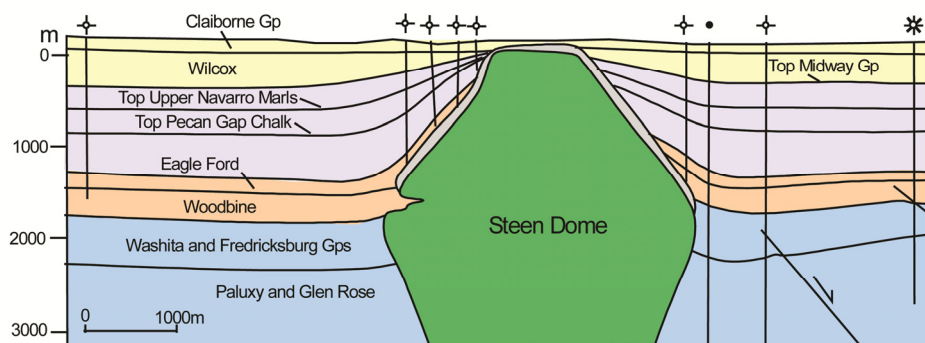
Butler Dome is located in the southern part of the central axis of the basin (Fig. 10), and is representative of a number of the domes in this area, including the Boggy Creek, Brooks, Pal-

estine, and Steen domes. Current interpretation is confined to the Glen Rose–Cotton Valley interval, but this geometry is only present up to the top of the Fredricksburg Group (Fig. 12A). Above this interval, within the Woodbine and Eagle Ford, the boundary tapers, suggesting that  $R_{sg}$  is less than  $R_a$ . This geometry is maintained within the Cretaceous chinks and the top of the diapir flattens within the Pecan Gap chalk. Because  $R_a$  values are believed to be lower within this interval, the  $R_{sg}/R_a$  ratio decreases more than  $R_a$  resulting in a decreasing  $R_{sg}/R_a$  ratio. As shown in Figure 9,  $R_{sg}/R_a$  values can be influenced both by changing  $R_{sg}$  and  $R_a$  values. The drop in  $R_{sg}$  resulting in tapering is most likely related to the depletion of the salt in the source layer. An additional observation is that the sediments within the tapered interval actually show an uplift associated with warping by the rising tapered diapir. Since upwarping represents the early stage of active diapirism, followed by piercement through a faulted crest, it is possible that part of the uplift of the tapered diapir occurred by active processes.

Experiment G1 illustrates the mechanism responsible for depleting source material in reducing  $R_{sg}$ , even if  $R_a$  is constant. As observed for the experiment the reduction in the rate of salt flow occurs long before the actual welding of the salt layer because of frictional resistance to Poiseuille flow along the top and bottom boundaries of the salt (Batchelor, 2000). However, be-



A



B

Figure 12. Cross sectional geometries for two diapirs along the central basin axis (modified after Wood and Giles, 1982; Seni and Jackson, 1982b). (A) Butler Dome and (B) Steen Dome.

cause of the spindle-shaped geometry of the diapir, the upwarp of the adjacent sediments is not apparent in the tapered stage.

### Steen Dome

Steen Dome is located in the northeast part of the central axis of the basin (Fig. 10). The geometry of the diapir is very similar to the Butler Dome, with a flared geometry to the top of the Fredericksburg, followed by a tapered geometry (Fig. 12B). The primary difference is that the tapered geometry extends into the Wilcox where the diapir is eclipsed. This implies a later depletion of the source layer compared to the Butler Dome. Significant warping of units between the Eagle Ford and Midway occurs during the uplift associated with the tapering stage. The west flank of the dome is marked by small interval of tapering and flare, confined to the Woodbine.

The dimensions of diapirs in the central part of the basin are generally greater than those on the flanks.

The Stein and Buler domes have diameters of approximately 2400 and 2800 m in the feeder. Both of these domes also have significantly larger salt volumes (areas in cross section) in the Glen Rose and higher units, compared to those in the flank regions. Similar values are found in other central domes such as Boggy Creek and Palestine.

The earlier tapering and eclipse of diapirs resulting in low  $R_{sg}/R_a$  values in the central part of the basin is enigmatic. This may be related to the greater thickness of the salt source layer and the larger dimensions of the diapirs. As shown in experimental models G6 and G8, thicker source layers result in diapirs with larger volumes and diameters. However, the larger rates of gross salt rise influenced by both the greater thickness of the source layer and the higher sedimentation rates in the central part of the basin may have resulted in rapid depletion of the source layer. This may have reduced the  $R_{sg}/R_a$  ratios, leading to earlier eclipse of the diapirs.

## CONCLUSIONS

Controlled experimental models provide key insights on the influence of different parameters on the geometry and progressive evolution of salt diapirs. The results of the models can be used to understand the evolution of natural salt diapirs in sedimentary basins.

Constant sedimentation rate experiments show that the evolution of diapirs is strongly dependent on the sediment load, rates of aggradation and the thickness of the source layer. Larger loads, lower rates of sedimentation and thicker source layers result in higher  $R_{sg}/R_a$  ratios leading to cylindrical diapirs, which eventually develop flared shapes with overhangs. Smaller loads, higher sedimentation rates and thinner source layers result in lower  $R_{sg}/R_a$  ratios leading to tapered shapes and eventual eclipse and occlusion of the diapirs.

Variable sedimentation rates result in changing shapes of diapirs over time. A small increase in sedimentation rates for flared or cylindrical diapirs result in an initial eclipse followed by tapering and a transition to active diapirism, enabling the diapir to pierce the overlying sediments. Subsequently, the narrower diapir continues to grow by passive diapirism. A large increase in rates result in a permanent eclipse, because the tapered diapir is unable to penetrate the greater thickness of the overburden. Thicker source layers generally result in higher rates of salt flow resulting in wider diapirs with larger salt volumes.

The models suggest that tapering and flaring are mechanisms for maintaining an equilibrium between net rates of sedimentation ( $R_a$ ) and salt rise ( $R_{sn}$ ), with changing  $R_{sg}/R_a$  values. Flaring is caused by high  $R_{sg}/R_a$ , but is also an effective mechanism of decreasing the rate of net salt rise by increasing the surface area of the top of the diapir. Tapering is caused by low  $R_{sg}/R_a$ , but is a mechanism for increasing the rate of salt rise by decreasing the diameter, thereby increasing the rate of salt rise to enable active piercement and continuing diapirism.

In the East Texas Basin, diapirs in the basin flanks, such as the Bethel and Oakwood domes, show the effects of increasing sediment load and varying sedimentation rates on diapir geometry. These diapirs exhibit cylindrical to flared geometries within the Cretaceous units followed by rapid tapering and flattening of the top of the diapir due to increased sedimentation rates in the early Tertiary. They typically have smaller diameters and salt volumes suggestive of thin source layers. On the other hand, the Butler and Stein domes, located along the central basin axis, while exhibiting early cylindrical to flared patterns, show early tapering and warping of sediments even during relatively low rates of sedimentation. They also exhibit larger diameters and salt volumes, suggesting the possibility of a depleted source layers during the later stages of formation.

The models are directly applicable to analyzing the geometry and evolution of poorly or partially imaged salt diapirs, and understanding the key factors controlling the rates of salt rise in subsurface examples from the East Texas Basin, the Gulf of Mexico, and other salt basins.

### ACKNOWLEDGMENTS

We thank reviewers Sandro Serra and Greg Schoenborn and editor Barry Katz for their constructive reviews, which helped improve the quality of the manuscript.

### REFERENCES CITED

- Barton, D. C., 1933, Mechanics of formation of salt domes with special reference to Gulf Coast salt domes of Texas and Louisiana: *American Association of Petroleum Geologists Bulletin*, v. 17, p. 1025–1083.
- Batchelor, G. K., 2000, An introduction to fluid dynamics: Cambridge University Press, U.K., 615 p.
- Bishop, R. S., 1978, Mechanism for emplacement of piercement diapirs: *American Association of Petroleum Geologists Bulletin*, v. 62, p. 1561–1583.
- Brun, J.-P., and X. Fort, 2011, Salt tectonics at passive margins: geology versus models: *Marine and Petroleum Geology*, v. 28, p. 1123–1145.
- Frey, M. G., and W. H. Grimes, 1970, Bay Marchand–Timbalier Bay–Caillou Island salt complex, Louisiana, in M. T. Halbouty, ed., *Geology of giant petroleum fields*: American Association of Petroleum Geologists Memoir 14, Tulsa, Oklahoma, Tulsa, Oklahoma, p. 277–291.
- Ge, H., M. P. Jackson, and B. C. Vendeville, 1997, Kinematics and dynamics of salt tectonics driven by progradation: *American Association of Petroleum Geologists Bulletin*, v. 81, p. 398–423.
- Gussow, W. C., 1968, Salt diapirism: Importance of temperature and energy source of emplacement, in J. Braunstein and G. D. O'Brien, eds., *Diapirism and diapirs*: American Association of Petroleum Geologists Memoir 8, Tulsa, Oklahoma, p. 183–214.
- Hudec, M. R., and M. Jackson, 2007, *Terra infirma*: Understanding salt tectonics: *Earth-Science Reviews*, v. 82, p. 1–28.
- Jackson, M. P. A., and S. J. Seni, 1984, Atlas of salt domes in the East Texas Basin: Texas Bureau of Economic Geology Report of Investigations 140, Austin, 102 p.
- Jenyon, M. K., 1986, Salt tectonics: Elsevier, London, U.K., 191 p.
- Johnson, A., 1970, Physical processes in geology: Freeman, Cooper and Company, San Francisco, California, 577 p.
- Jackson, M. P. A., B. C. Vendeville, and D. Schultz-Ela, 1994, Structural dynamics of salt systems: *Annual Review of Earth and Planetary Sciences*, v. 22, p. 93–117.
- Jackson, M. P. A., D. G. Roberts, and S. Snelson, eds., 1995, Salt tectonics: A global perspective: American Association of Petroleum Geologists Memoir 65, Tulsa, Oklahoma, 454 p.
- Loocke, J. E., 1978, Growth history of the Hainesville Salt Dome, Wood County, Texas: M.S. Thesis, University of Texas at Austin, 95 p.
- Nettleton, L. L., 1934, Fluid mechanics of salt domes: *American Association of Petroleum Geologists Bulletin*, v. 81, p. 1175–1204.
- Schultz-Ela, D. D., M. P. Jackson, and B. C. Vendeville, 1993, Mechanics of active salt diapirism: *Tectonophysics*, v. 228, p. 275–312.
- Seni, S., and M. P. A. Jackson, 1983a, Evolution of salt structures, East Texas Diapir Province, part 1: Sedimentary record of halokinesis: *American Association of Petroleum Geologists Bulletin*, v. 67, p. 1219–1244.
- Seni, S., and M. P. A. Jackson, 1983b, Evolution of salt structures, East Texas Diapir Province, part 2: Patterns and rates of halokinesis: *American Association of Petroleum Geologists Bulletin*, v. 67, p. 1245–1274.
- Talbot, C. J., 1995, Molding of salt diapirs by stiff overburden, in M. P. A. Jackson, D. G. Roberts, and S. Snelson, eds., 1995, Salt tectonics: A global perspective: American Association of Petroleum Geologists Memoir 65, Tulsa, Oklahoma, p. 61–75.
- Trusheim, F., 1960, Mechanism of salt migration in northern Germany: *American Association of Petroleum Geologists Bulletin*, v. 44, p. 1519–1540.
- Vendeville, B., and M. Jackson, 1992a, The rise of diapirs during thin-skinned extension: *Marine and Petroleum Geology*, v. 9, p. 331–354.
- Vendeville, B., and M. Jackson, 1992b, The fall of diapirs during thin-skinned extension: *Marine and Petroleum Geology*, v. 9, p. 354–371.
- Weijermars, R., M. P. A. Jackson, and B. Vendeville, 1993, Rheological modeling of salt provinces: *Tectonophysics*, v. 217, p. 143–174.
- Warsitzka, M., J. Kley, and N. Kukowski, 2013, Salt diapirism driven by differential loading—Some insights from analogue modelling: *Tectonophysics*, v. 591, p. 83–97.
- Wood, D. H., and A. B. Giles, 1982, Hydrocarbon accumulation patterns in the East Texas Salt Dome Province: Texas Bureau of Economic Geology Geological Circular 82–6, Austin, 36 p.